Inelastic Deformation and Damage Evolution of Light Alloys under Dynamic Punching

Vladimir V. Skripnyak[1, a)], Natalia V. Skripnyak[1, b)], Maxim O. Chirkov[1,c)] and Vladimir A. Skripnyak[1,d)]

[1]*National Research Tomsk State University, 36 Lenin Avenue, Tomsk, Russia, 634050*

[a)] Corresponding author: skrp2012@yandex.ru
[b)] natali.skrp@mail.ru,
[c)] sashakir94@mail.ru,
[d)] skrp2006@yandex.ru

Abstract. The results of research of mechanisms of nucleation and growth of damage of aluminum-magnesium or magnesium alloys during dynamic stamping and new obtained experimental data for modification of the constitutive and damage models are presented. The relevance of the research performed is due to the need achieving of high accuracy and adequate computer designing methods for predicting possible damage of construction under manufacturing or exploitation loadings of lightweight structures of transport equipment, space and aircraft from aluminum-magnesium and magnesium alloys with increased specific strength. The deformation and crack formation under high-velocity punching of a steel indenter to plates made of AMg2 aluminum-magnesium alloys and MA2-1 magnesium alloy were simulated using the LS DYNA solver (ANSYS WB 19.2).

INTRODUCTION

Light alloys have low mass density, high specific strength characteristics, high mechanical damping properties, electromagnetic shielding capacity, high thermal conductivity, which makes them promising structural materials that can significantly reduce the weight of structures [1,2].

In this regard, an important task is to obtain information on the mechanical behavior of structural light alloys in a wide range of loading conditions, including dynamic effects. It should be noted that magnesium alloys belong to the isomechanical subgroup of alloys with a hexagonal close-packed crystal lattice (HCP), the mechanical behavior of which differs from the behavior of other subgroups of HCP alloys [3]. To improve the accuracy of theoretical predictions obtained using numerical modeling of the mechanical behavior (deformation and fracture) of magnesium alloys under impact conditions, it is necessary to modify the governing equations and models of damage initiation and fracture [4, 5].

One of the important aspects of describing the mechanical behavior of deformable magnesium alloys under high-speed deformation of products is predicting the localization of plastic deformation and the development of damage. Studies have shown that both the equivalent strain rate and the stress state triaxiality parameter ($\eta = -p/\sigma_{eq}$, where p is the pressure and σeq is the equivalent von Mises stress) have a significant effect on the conditions of damage and fracture of magnesium and aluminum alloys during high-speed deformation under punching [6].

The aim of this work was to study the mechanical behavior of thin-sheet rolled AMg2 and MA2-1 alloys under biaxial tension during punching with a hemispherical indenter.

The results of experimental and theoretical studies of the mechanical behavior of magnesium and aluminum alloys at high strain rates obtained in the work complement the data obtained earlier.

MATERIALS AND TESTING

Tests on biaxial tension during punching by a hemispherical indenter of AMg2 aluminum alloy (Al 1520) and industrial magnesium MA2-1 (Mg–3Al–1Zn) alloy samples were carried out in accordance with ISO 8490-86 and ASTM E643-09 standards, as well as with INSTRON recommendations. The samples deformation, damage and fracture were studied under punching at velocities 0.1 ± 0.001 m/s, 1 ± 0.01 m/s, 5 ± 0.01 m/s and 10 ± 0.1 m/s. Changes of the force acting on the indenter, as well as maximum displacements in the contact zone during the tests were recorded with high time resolution. The load was recorded using a certified dynamic Kistler sensor. A force sensor was installed in the indenter, and the sample was fixed in a clamping device moving at a specified speed. Five tests were done for each punching velocity. The rigidity of the Instron VHS 40/50-20 high-speed servo hydraulic test bench and the sample movement speed control system ensured loading of the samples with a high degree of constancy of the specified indentation speeds. The indenter movement speeds were recorded with a time resolution of 0.0001 s until the samples failed.

Industrial rolled polycrystalline aluminum alloy AMg2 (Al 1520 accordingly of GOST 17232–99) had the following chemical composition (wt.%): 2.2 % Mg, 0.06 % Mn, 0.5 % Fe, 0.4 % Si, 0.1 % Cu, Al – the rest, and the average grain size was equal to 40 ± 10 μm. Industrial rolled polycrystalline MA2-1 (Mg-3Al-1Zn) alloy have the chemical composition (wt. %): 93.7 % Mg, 4.36 % Al, 1.34 % Zn and 0.39 % Mn, and the average grain size was equal to 80 ± 10 μm.

The mass density of MA2-1 alloy was 1.79 g/cm3, under quasi-static loads at a temperature of 295 K, the alloy with an average grain size of 40 μm had a yield strength of $\sigma_{0.2}$ = 150 MPa, tensile strength UTS = 260–280 MPa, elongation before failure δ ~ 5…12%.

At the room temperature MA2-1 alloy have the shear modulus μ = 17 GPa, the Young's modulus E = 44.55 GPa, the Poisson's ratio υ = 0.35, the quasistatic yield strength $\sigma_{0.2}$ = 150 ±5 MPa, the tensile strength σ_{UTS} = 250±10 MPa, the linear thermal expansion coefficient 26•10-6 K^{-1}, specific heat capacity C_p= 1088.5 J/(kg•K), and Taylor-Quinney coefficient β ≈ 0.4…0.6 [7].

The samples of MA2-1 with the thickness of 2.0 ± 0.01 mm for the biaxial tensile under punching tests with a hemispherical indenter were cut perpendicular to the axis of symmetry from the rod with a diameter of 60 mm by the electro erosion method. The samples of AMg2 with the thickness of1.05 ± 0.05 mm and 60±0.2 mm diameter for punching by a hemispherical indenter were cut by the electro erosion method from thin sheet of the alloy.

Reducing the coefficient of friction between the samples and the indenter during punch tests was achieving by the surfaces of the samples was polished and using oil lubricant. IPF ER-3 lubricant (OOO Gazpromneft - lubricant, Moscow, Russia) was used between the indenter and the sample surface; it significantly reduces friction during stamping and has anti-seize properties.

NUMERICAL SIMULATION

Numerical modeling of plastic flow and damage development of alloys under dynamic punching of plates by a hemispherical indenter was carried out using the original UMAT module in the LS DYNA complex in ANSYS WB 19.2. The mechanical response of plates under punching described by the system of equations according the Lagrangian approach includes conservation equations of isotropic continual medium, kinematic relations, constitutive relations [8], relaxation equation for the deviator stress tensor [3], plastic potential in the modified Gurson-Tvergaard-Nedleman's form [9], thermodynamic relations of determination of temperature changes during high strain rate deformation of alloys, Nedleman's damage kinetics equations [10].

The flow stress of the alloy during damage development was described using the constitutive relation [9]:

$$(\sigma_{eq}^2/\ \sigma_s^c\sigma_s^t) + 2q_1\ g^*\cosh[-q_2\ p/(2\ \sqrt{\sigma_s^c\sigma_s^t})]+(1\ -g^*)[3(\sigma_s^c - \sigma_s^t)/\sigma_s^c\ \sigma_s^t]p\text{-}1\text{-}(\ q_3(g^*)^2 = 0, \quad (1)$$

where σ_{eq} is the equivalent von Mises stress, σ^c_s is the yield strength under compression, σ^t_s is the yield strength under tension, p is the pressure, q_1, q_2 and q_3 are the model parameters, and g* is the material damage parameter.

The material in the contact zone with the punch interaction of plate is deformed under compression, while on the back side of the plate, the material is under tension.

Since magnesium alloys exhibit significant asymmetry in their resistance to plastic deformation under compression and tension, the plastic potential was adopted in the form (1).

Aluminum alloys exhibit very slight asymmetry in their resistance to plastic deformation under compression and tension. If the alloy's yield strengths under tension and compression are the same, equation (1) is reduced to the traditional Gurson-Tvergaard-Needleman form [10].

A modification of the Zerilli-Armstrong equation of state for magnesium alloys with an HCP lattice to describe the dependence of σs on the strain rate, equivalent plastic strain and temperature was used in the form (3) [8]:

$$\sigma_s = \sigma_{s0} + C_5(\varepsilon_{eq}^p)^n + C_2 \exp\{-C_3 T + C_4 T \ln(\dot{\varepsilon}*)\}, \quad (2)$$

where σ_{s0}, k_{hp}, n_1, C_2, C_3, C_4, C_5 are the material parameters for tension and compression, T is the temperature, $\varepsilon^* = \dot{\varepsilon}_{eq}^p / \dot{\varepsilon}_{eq0}$, $\dot{\varepsilon}_{eq}^p = [(2/3)\dot{\varepsilon}_{ij}^p \dot{\varepsilon}_{ij}^p]^{1/2}$, $\dot{\varepsilon}_{eq0} = 1 s^{-1}$.

The model parameters for the MA2-1 and AMg2 alloys are shown in Table 1.

TABLE 1. Model coefficients for MA2-1 and AMg2 alloys

Coefficient	σ_{s0}, MPa	C_2, MPa	C_3, K^{-1}	C_4, K^{-1}	C_5, MPa	n_1
MA2-1 (tension)	60	120	0.016	0.00178	396	0.17
MA2-1 (compression)	102	60	0.016	0.00178	57600	2
AMg2	1.51	495	0.0034	0.00012	175	0.278

The temperature increment during plastic flow due to energy dissipation was determined in the adiabatic approximation [3]

$$T = T_0 + \int_0^{\varepsilon_{eq}^p} (\beta/\rho\ C_p)\ \sigma_{eq}\, d\,\varepsilon_{eq}^p, \quad (3)$$

where T_0 is the initial temperature, β~0.47 is the Taylor-Quinney coefficient for MA2-1 [7] and β~0.9 for AMg2, and the equivalent von Mises stress is $\sigma_{eq} = [(3/2)\sigma_{ij}\,\sigma_{ij} - 0.5\,\sigma^2_{kk}]^{1/2}$, σ_{ij} are the stress tensor components, ρ is the mass density, C_p is the specific heat at constant pressure, $\varepsilon_{eq}^p = [(2/3)\varepsilon_{ij}^p \varepsilon_{ij}^p]^{1/2}$ is the equivalent plastic strain.

The decreasing of the resistance to plastic flow caused by heating as a result of dissipation of stress work on plastic deformations affects the occurrence of localization of plastic flow and the subsequent growth of the damage parameter in the material. The increment of the damage parameter over time, caused by the origin of damage, depends on the equivalent plastic deformation ε_{eq}^p and is described using a normal distribution. The growth rate of the damage parameter caused by the increasing in the size of damages is associated with volumetric inelastic deformations.

The Gurson-Tvergaard-Needleman (GTN) ductile fracture model requires knowledge of 9 coefficients: three model coefficients (q_1, q_2, and q_3), the initial damage fraction f_0, three damage kinetics coefficients (ε_N, s_N, and f_N), and two fracture coefficients (f_c and f_F) [8]. In the model, damage initiation in a material is determined by ε_N and sN coefficients dependent on the inelastic strain distribution in deformed body. In this study, it was assumed that damage initiation in plates under punching begins in the formed bands of plastic strain localization. The final stage of ductile fracture consist of coalescence of damage in the fracture zone into a crack, which leads to an acceleration of the growth rate of the damage parameter g* up to fracture when the damage parameter reaches the f_F value.

The Considere's criterion [11] was used as a criterion for the origin of plastic deformation instability leading to the formation of macro localization bands:

$$\frac{\partial \sigma_s}{\partial \varepsilon_{eq}^p} + \frac{\partial \sigma_s}{\partial \dot{\varepsilon}_{eq}^p}\frac{\partial \dot{\varepsilon}_{eq}^p}{\partial \varepsilon_{eq}^p} + \frac{\partial \sigma_s}{\partial T}\frac{\partial T}{\partial \varepsilon_{eq}^p} + \frac{\partial \sigma_s}{\partial\, g*}\partial\frac{g*}{\partial \varepsilon_{eq}^p} = \sigma_s, \quad (4)$$

where g* is the damage parameter of the alloy.

Criterion (4) takes the form (5) in the initial state taking into account (1)–(3), under loading at a constant deformation rate, in the absence of damage in the alloy:

$$\frac{\partial \sigma_s}{\partial \varepsilon_{\text{eq}}^p} = (1 - \frac{\partial \sigma_s}{\partial T} \frac{\beta}{\rho C_p}) \sigma_s \,, \tag{5}$$

The values of the coefficients were determined taking into account the experimental data [12-14] for magnesium alloy.The model parameters for MA2 alloy were obtained in a semi-inverse numerical simulation of a uniaxial tensile test: $q_1 = 1.5$, $q_2 = 1$, $q_3 = 1.0$, $f_0 = 0$, $f_N = 0.156$, $f_c = 0.112$, $f_F = 0.260$, $\varepsilon_N = 0.1$, $s_N = 0.02$.

The model parameters for the AMg2 alloy were obtained in a semi-inverse numerical simulation of a uniaxial tensile test: $q_1 = 1.5$, $q_2 = 1$, $q_3 = 2.25$, $f_0 = 0$, $f_N = 0.136$, $f_c = 0.02$, $f_F = 0.03$, $\varepsilon_N = 0.26$, $s_N = 0.1$.

In modeling the punching of plates by a hemispherical indenter, boundary conditions (9) specified on the surfaces shown in Fig. 1 were used.

The surface of the hemispherical indenter is designated S_1. The fixed parts of the specimen surface between the upper and lower support matrices are designated S_2, S_3, and S_4, respectively. The lower part of the specimen surface S_5 is the free surface, and the changing contact surface between the specimen and the indenter is designated S_6.

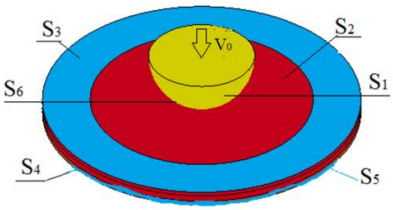

FIGURE 1. Surface numbering scheme for formulating boundary conditions for pushing by a hemispherical indenter

The boundary conditions are as follows for high-velocity pressing of a flat sample by a hemispherical indenter:

$$u_3|_{S_6} = V_0, u_i|_{S_3 \cup S_4} = 0, i = 1,2,3 \,, \sigma_{ij}|_{S_5} = 0, \sigma_{ij}|_{S_2 \cap S_6} = 0,$$
$$u_{i^+}|_{S_6} = u_{i^-}|_{S_6} \,, p^+|_{S_6} = -p^-|_{S_6} \,, \sigma_{ij^+}|_{S_6} = \sigma_{ij^-}|_{S_6} = 0, i \neq j, \tag{5}$$

where u_3 are the components of the particle velocity vector on the surface S_k, k=1…6, σ_{ij} are the stress tensor components, p is the pressure, V_0 is the velocity of the rigid stamp.

It was assumed that at the initial moment of time the sample material was in a uniform temperature field in an unstressed state. The contact conditions of the interaction of the indenter with the sample and the clamping device with the sample were described using the model implemented in the automatic_surface_to_surface LS DYNA map. The friction coefficient parameters were set at $F_S = 0.4$, and the damping coefficients were $V_{DC} = 30$, which ensured the absence of oscillations of the calculated forces in the contact zone. A second-order finite-difference scheme with a characteristic spatial grid step size of 0.3 mm was used in the calculations. Three-dimensional linear hexagonal elements (~200,000 elements) were used to discretize the calculated region of the sample. The indenter and clamping device elements were modeled as rigid bodies. The selected step of the spatial grid ensured the convergence of the numerical simulation results.

RESULTS AND DISCUSSION

Experimental force resistance curves to punching versus the deflection $F(u_3)$ for velocities from 0.1 to 10 m/s are shown in Fig. 2. The patterns of dependence of the punching force on the deflection, shown in Fig. 2, are preserved for the entire investigated range of punching velocities for MA2-1 and AMg2.

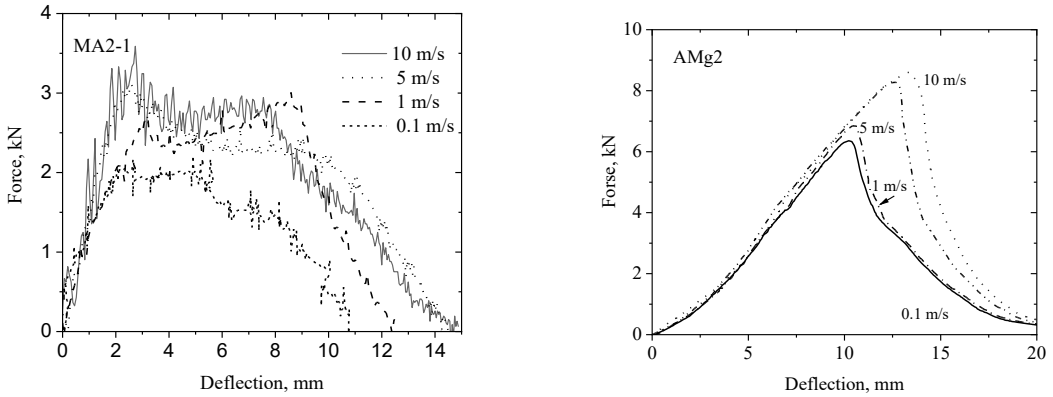

(a) (b)

FIGURE 2. (a) Experimental diagrams $F(u_3)$ for MA2-1 alloy, and (b) for AMg2

The obtained results indicate that in the considered range of loading rates from 0.1 to 10 m/s, viscous fracture is realized in the MA2-1 alloy under deformation conditions during punching. The formation of cracks is preceded by significant equivalent plastic deformation.

The oscillations of the punching forces observed in Fig. 2(a) are caused by the relaxation of tangential stresses during the nucleation of localized shear micro bands at high deformation rates of the magnesium alloy. The strain rates increase with increasing punching rate, which is accompanied by an increase in the oscillation amplitude. It should be noted that the use of a special lubricant in the contact zone of the indenter and sample surfaces not only reduces friction forces, but also contributes to an increase in the deflection of the sample before the moment of crack nucleation.

Figure 4 shows photographs of MA2-1 samples after punching with a hemispherical indenter at speeds of 10, 5, 1 and 0.1 m/s, respectively.

The shape of the cracks in the indentation zone depends on the indentation velocity and the thickness of the specimens. At an indentation velocity of 10 m/s, all tested specimens of the MA2-1 alloy with a thickness of 2 mm developed only radial cracks, which led to the opening of 4 fragments. No circumferential cracks were observed. At lower indentation velocities, three radial cracks were formed, which led to the opening of 3 fragments, as can be seen in Fig. 3.

The results of numerical modeling of the conditions of high-speed indentation of MA2-1 alloy plates showed that the strength under biaxial tension is 0.24 GPa at an indentation velocity of 10 m/s, and 0.17 GPa at a velocity of 0.1 m/s. The obtained estimates of the tensile strength of the MA2-1 alloy under dynamic indentation are consistent with the data [1, 9, 10] obtained under uniaxial tension. The values of ultimate deformations before failure under biaxial tension under punching were found to be significantly lower than under uniaxial tension.

Thus, for the MA2-1 alloy in the failure zone of samples under biaxial tension under dynamic punching, the value of plastic deformation is significantly lower than the values of residual elongation δ under uniaxial tension at strain rates of 0.1, 10^2 and 10^3 s^{-1} and an initial temperature of 295 K.

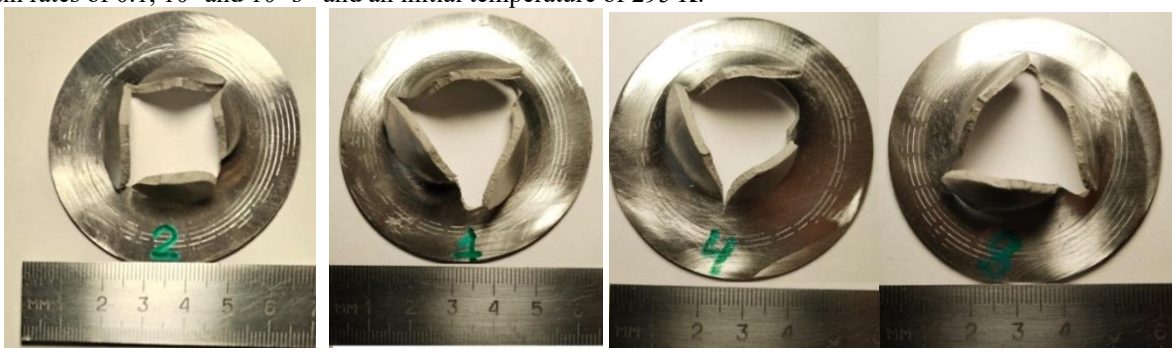

(a) (b) (c) (d)

FIGURE 3. Photographs of the samples after indentation with the hemispherical punch at velocities of (*a*) 10, (*b*) 5, (*c*) 1, and (*d*) 0.1 m/s

Figure 3 shows photographs of AMg2 samples after punching with a hemispherical indenter at speeds of 10, 5, 1 and 0.1 m/s, respectively. The shape of the cracks in the indentation zone depends on the indentation velocity and the thickness of the specimens.

(a) (b) (c) (d)

FIGURE 4. Photographs of the samples after indentation with the hemispherical punch at velocities of (a) 10, (b) 5, (c) 1, and (d) 0.1 m/s

Figure 5 shows the calculated and experimental dependences of force on deflection at an indentation speed of 10 m/s. Curve 1 corresponds to the calculated values, and curve 2 to the experimental ones.

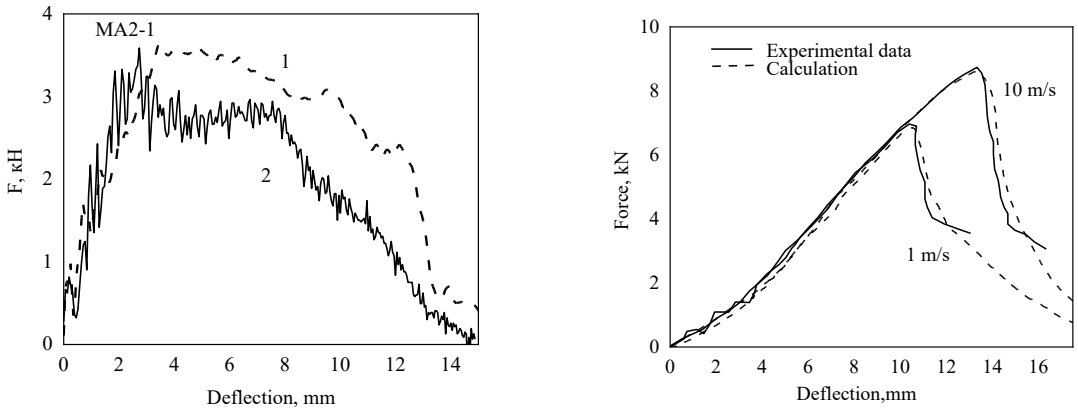

(a) (b)

FIGURE 5. *a*) Calculated and experimental dependences of the force on deflection at an indentation velocity of 10 m/s; curve 1 corresponds to calculation result, and 2 is experimental data; (*b*) Calculated and experimental force $F(u_z)$ versus deflection curves for punching through aluminum plates of alloy AMg2 by a hemispherical indenter with a diameter of 20 mm

The simulation results indicate that the distribution of equivalent plastic strain is non-uniform across the plate thickness during dynamic punching as MA2-1 as AMg2 plates with a hemispherical indenter. The calculated distribution of the equivalent plastic strain and equivalent Mises stress in the cross section of AMg2 samples is shown in Fig. 6**.**

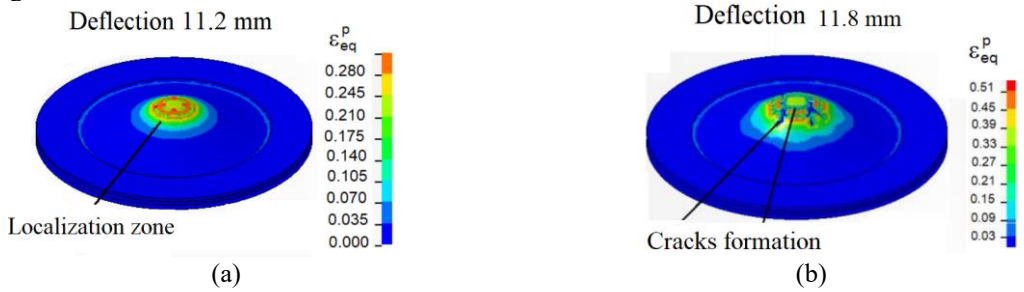

(a) (b)

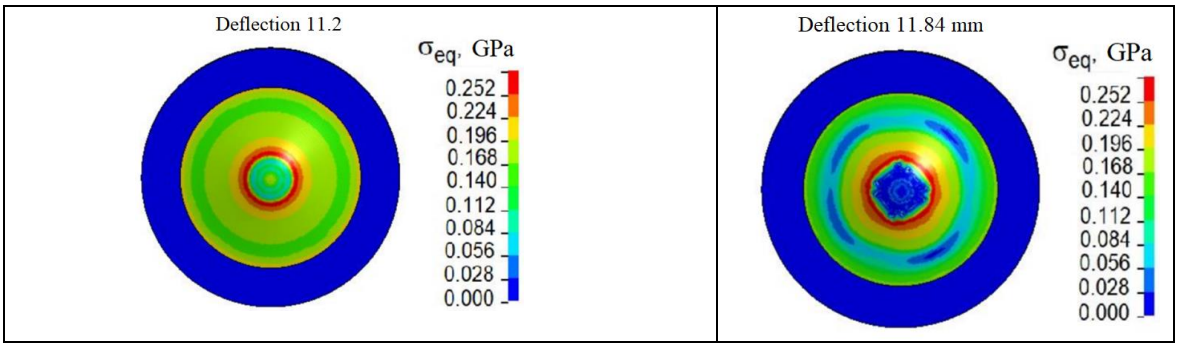

(c) (d)

FIGURE 6. Calculated distribution of the equivalent plastic strain at the back surface of AMg2 plate at the punching velocity of 10 m/s (a, b); (Calculated distribution of equivalent Mises stress at the back surface of the punched samples (c,d)

The maximum values of equivalent plastic strain are achieved during stretching of the material in the near-surface layer on the back surface of the loaded plate. Therefore, during punching, cracks initiate precisely from the back surface of the plates, which leads to the formation of a system of cracks with increasing strain. The experimental and calculated dependences of the punching force on the deflection have a good correlation at the velocities of 0.01, 0.1, 1, 5 and 10 m/s.

The simulation results indicate that the distribution of equivalent plastic strain is essentially non-uniform across the plate thickness during dynamic punching of MA2-1 alloy plates with a hemispherical indenter. The calculated distribution of the equivalent plastic strain and equivalent Mises stress in the cross section of the deformed MA2-1 sample at the time of 0.202 ms is shown in Fig. 7(a) and Fig. 7(b) respectively.

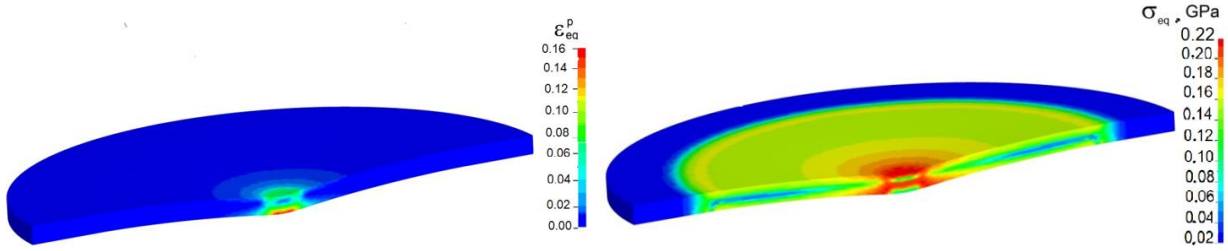

(a) (b)

FIGURE 7. (a) Calculated distribution of the equivalent plastic strain in the cross section of MA2-1 samples at a time instant of 0.202 ms with an indentation velocity of 10 m/s; (b) Calculated distribution of equivalent Mises stress at time of 0.202 ms

The obtained results explain the reasons for the absence of the formation of a system of circular cracks during dynamic loading of magnesium alloy plates. The calculated distribution of the equivalent von Mises stress in the cross section of the MA2-1 alloy sample during punching at a time of 0.202 ms is shown in Fig. 7(b).

The calculated distributions of equivalent stresses in the plate cross-section during punching indicate that near the middle surface the shear stresses are significantly lower than on the contact and back free surfaces of the plate.

The relatively low friction on the contact surfaces taken into account in the calculation model does not introduce significant distortions into the calculated distributions of equivalent von Mises stresses and does not cause changes in the nature of crack initiation. No initiation of brittle micro cracks is observed.

The evolution of equivalent stresses and equivalent plastic strains corresponds to the viscous nature of fracture of magnesium alloy plates in the studied range of punching speeds up to 10 m/s. The obtained results indicate the potential possibility of using dynamic stamping for the production of products from sheet rolled magnesium alloy MA2-1. The calculated distribution of effective strain rates in the cross section of MA2-1 alloy samples after punching at a speed of 10 m/s are shown in Fig. 8 at a time of 0.202 ms (a); at a time of 0.606 ms (b). Note that the configuration of forming cracks obtained in the calculations agrees with the experimental results shown in Fig. 4.

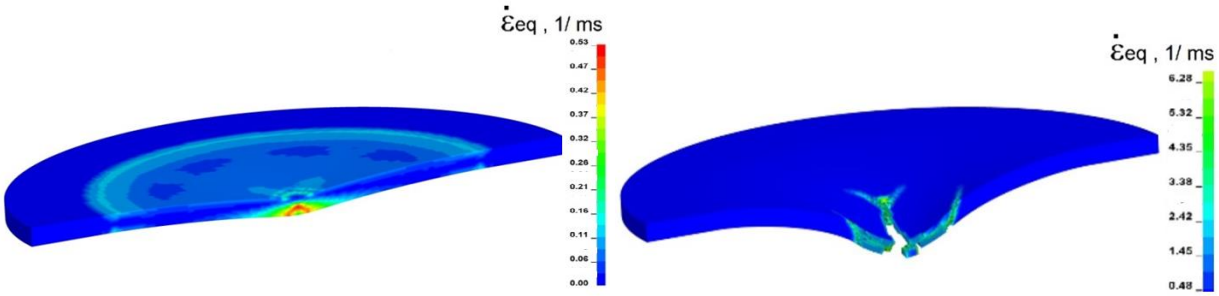

(a) (b)

FIGURE 8. Calculated distribution of effective strain rates in the cross section of MA2-1 samples with an indentation velocity of 10 m/s at time instants of (*a*) 0.202 and (*b*) 0.606 ms

The strain rate in the plastic deformation zone during punching at a speed of 10 m/s varies in the range from 100 to 530 s^{-1}. The strain rate in the local zone near the crack formation can achieved up to ~6300 s−1. Thus, to improve the accuracy of predictions of the mechanical behavior of the magnesium alloy MA2-1 (damage and residual stresses) obtained as a result of numerical modeling of dynamic punching of plates, it is necessary to use wide-range governing equations and kinetic models of damage and fracture of alloys that take into account the influence of loading parameters such as temperature, strain rate, plastic deformation value, stress triaxiality parameter, as well as structural factors, including grain structure parameters. The calculated distribution of the stress state triaxiality parameter in the cross section of the MA2-1 alloy specimens at a time of 0.202 ms at an indentation speed of 10 m/s is shown in Fig. 9.

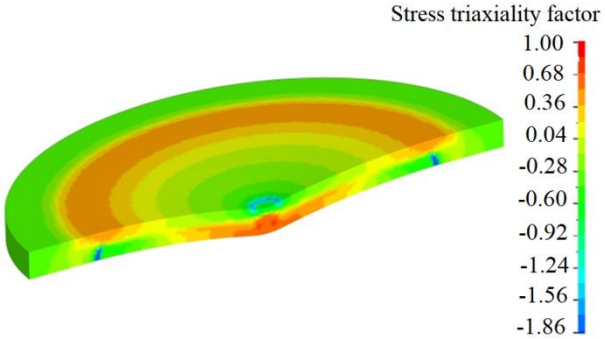

FIGURE. 9. Calculated distribution of the stress triaxiality in the cross-section of the MA2-1 sample during indentation at a time instant of 0.202 ms

The obtained results of numerical modeling of high-speed punching of MA2-1 alloy plates with a hemispherical indenter indicate that the plate material is deformed under stress states that change in the plate volume during deformation. Note that at the initial stages of plate deflection, the material was deformed at negative and positive values of the stress triaxiality parameter, which is due to the tensile and compressive states in the plate layers during deflection. The stress state in the zone of the deformable plate near the forming cracks changes, which leads not only to a change in the absolute values of the stress state triaxiality parameter, but also to a change in its sign. Therefore, the resulting effect of the stress triaxiality parameter on the strain before failure decreases with increasing strain rates under biaxial tension during dynamic punching.

CONCLUSION

An experimental and theoretical research of the deformation and fracture processes of magnesium alloy MA2-1 and aluminum alloy AMg2 were carried out under biaxial tension during punching with a hemispherical indenter at speeds of 0.1, 1, 5 and 10 m/s at room temperature.

The results obtained indicate that for the MA2-1 alloy, the equivalent plastic strains at which damage accumulation begins are close to the values of the onset of plastic flow instability and decrease with an increase in the tensile strain rate from 0.1 to 1000 s^{-1}. It was shown that for the MA2-1 alloy in the considered range of loading rates from 0.1 to 10 m/s, ductile fracture occurs during deformation under punching.

The results obtained in this work indicate that for the magnesium alloy MA2-1 under biaxial tension under punching, the plastic deformation in the fracture zone of the sample is significantly lower than the values of residual elongation before fracture under uniaxial tension with strain rates of 0.1, 10, 100 and 1000 s-1 and initial room temperature.

It was shown that the evolution of equivalent stresses and equivalent plastic strains corresponds to the ductile nature of fracture of magnesium alloy plates in the studied range of punching rates.

The strains before fracture of magnesium alloy under biaxial tension under punching increases with increasing strain rate.

The obtained results of numerical modeling of high-speed punching of MA2-1 alloy plates with a hemispherical indenter indicate that the plate material is deformed under stress states that change in the plate volume during deformation. The effect of the stress triaxiality parameter on deformation before failure decreases with increasing deformation rates.

The obtained results indicate the potential possibility of using dynamic stamping for the production of products from sheet rolled magnesium alloy MA2-1. The research results obtained in this paper can be used in the development and modification of computational models of the mechanical behavior of magnesium alloy structures that are subject to plastic deformation under dynamic effects.

It is shown that under high-speed tension, ductile fracture of aluminum alloy AMg2 occurs as a result of damage initiation and growth in the zones of plastic deformation localization.

ACKNOWLEDGMENTS

The work was supported by the Russian Science Foundation: project 24-79-10103. The authors thank the Russian Science Foundation for research support.

REFERENCES

1. J. Yang, Z. Zhu, S. Han, Y. Gu, Z. Zhu, H.-D. Zhang, Evolution, limitations, advantages, and future challenges of magnesium alloys as materials for aerospace applications. J. Alloy. Compd. **1008**, 176707 (2024). https://doi.org/10.1016/j.jallcom.2024.176707
2. M. Yang, C. Chen, D. Wang, Y. Shao, W. Zhou, C. Shuai, Y. Yang, X. Ning, Biomedical rare-earth magnesium alloy: Current status and future prospects. J. Magnes. Alloy **12**, 1260–1282 (2024). https://doi.org/10.1016/j.jma.2024.03.014
3. V.V. Skripnyak, V.A Skripnyak, Hexagonal close-packed (hcp) alloys under dynamic impacts. J. Appl. Phys. **131**, 165902 (2022). https://doi.org/10.1063/5.0085338
4. J. Wang, X. Yuan, P. Jin, H. Ma, B. Shi, H. Zheng, T. Chen, W. Xia, Study on modified Johnson-Cook constitutive material model to predict the dynamic behavior Mg-1Al-4Y alloy Mater. Res. Express **7**, 026522 (2020). https://doi.org/10.1088/2053-1591/ab7070
5. J. Luan, C. Sun, X. Li, Q. Zhang, Constitutive model for AZ31 magnesium alloy based on isothermal compression test. Mater. Sci. Technol. **30**, 211–219 (2014). https://doi.org/10.1179/1743284713Y.0000000341
6. X. Huang, J. Hou, B. Lin, B. Li, B. Jiang, Deformation localization behavior research of AZ31 magnesium alloy under impact load. J. Phys. Conf. Ser. **2541**, 012054 (2023). https://doi.org/10.1088/1742-6596/2541/1/012054
7. N. A. Ozdur, S. C. Ermana, R. Seghir, L. Stainier, C.C. Aydıner, A thermomechanical investigation of textured magnesium in an effort to validate crystalplasticity simulations. Procedia Structural Integrity IWPDF 2023, 61, 277–284 (2024) Procedia Structural Integrity. **61**. pp. 277–284. https://doi.org/10.1016/j.prostr.2024.06.035
8. F.J. Zerilli, R.W. Armstrong, Constitutive equation for h.c.p. metals and high strength alloy steels. High strain rate effects on polymer, metal and ceramic matrix composites and other advanced materials. ASME **48**, 121–126 (1995).
9. X. Zhu,·Y. Lei, H. Wan,· S. Li, G. Dui Constitutive modeling of porosity and grain size effects on superelasticity of porous nanocrystalline NiTi shape memory alloy. Acta Mechanica. **234**, 6499 – 6513 (2023). https ://doi.org /10.1007/s00707-023-03721-0
10. A. Needleman, V. Tvergaard, Analyses of plastic flow localization in metals. Appl. Mech. Rev. **45**, S3–S18 (1992). https://doi.org/10.1115/1.3121390
11. I.S. Yasnikov, A. Vinogradov, Y. Estrin, Revisiting the Considère criterion from the viewpoint of dislocation theory fundamentals. Scr. Mater. **76**, 37–40 (2014). https://doi.org/10.1016/j.scriptamat.2013.12.009

12. P. Lukas, Z. Trojanova, Effect of fabrication processing on the deformation behaviour of AZ31 magnesium alloys. Kovove Mater. **49**, 385–391 (2011). https://doi.org/10.4149/km-2011-6-385
13. V.A. Skripnyak, V.V. Skripnyak, A.A. Kozulin, K.V. Iokhim, The influence of stress concentrators on the magnesium alloy mechanical behavior under deformation at high strain rates in the temperature range from 295 to 673 K. PNRPU Mechanics Bulletin **1**, 151–160 (2019). https://doi.org/10.15593/perm.mech/2019.1.13
14. S. Kurukuri, M.J. Worswick, D. Ghaffri Tari, R.K. Mishra, J.T. Carter, Rate sensitivity and tension–compression asymmetry in AZ31B magnesium alloy sheet. Phil. Trans. R. Soc. A. **372**, 20130216. (2014). http://dx.doi.org/10.1098/rsta.2013.0216